JACS
JOURNAL OF THE AMERICAN CHEMICAL SOCIETY
pubs.acs.org/JACS
Article

$[K_2(Bi@Pd_{12}@Bi_{20})]^{4-}$: An Endohedral Inorganic Fullerene with Spherical Aromaticity

Cong-Cong Shu, Dariusz W. Szczepanik, Alvaro Muñoz-Castro, Miquel Solà, and Zhong-Ming Sun*

Cite This: J. Am. Chem. Soc. 2024, 146, 14166−14173
Read Online
ACCESS | Metrics & More | Article Recommendations | Supporting Information

ABSTRACT: Inorganic fullerene clusters have attracted widespread attention due to their highly symmetrical geometric structures and intrinsic electronic properties. However, cage-like clusters composed of heavy metal elements with high symmetry are rarely reported, and their synthesis is also highly challenging. In this study, we present the synthesis of a $[K_2(Bi@Pd_{12}@Bi_{20})]^{4-}$ cluster that incorporates a $\{Bi_{20}\}$ cage with *pseudo*-I_h symmetry, making it the largest main group metal cluster compound composed of the bismuth element to date. Magnetic characterization and theoretical calculations suggest that the spin state of the overall cluster is a quartet. Quantum chemical calculations reveal that the $[Bi_{20}]^{3-}$ cluster has a similar electronic configuration to C_{60}^{6-} and the $[Bi@Pd_{12}@Bi_{20}]^{6-}$ cluster exhibits a unique open-shell aromatic character.

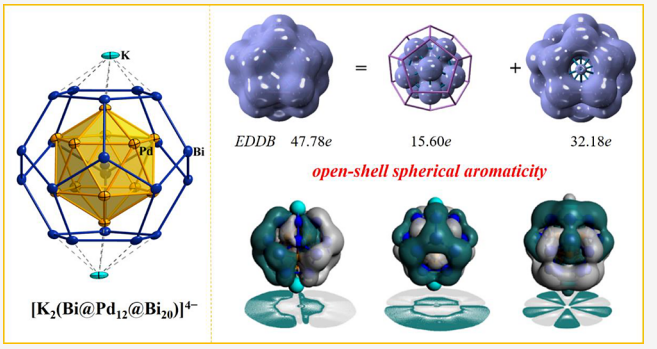

INTRODUCTION

The investigation of three-dimensional (3D) aromaticity in spherical molecules has deepened our understanding of their stability and reactivity.[1−7] Lipscomb's study on the structure of $B_{10}H_{10}^{2-}$ extended the research scope of aromaticity to 3D systems.[8,9] Subsequently, Wade and Mingos investigated the relationship between the structure types and the number of bonding electrons of boranes and carboranes, proposing simple rules of $2N + 2$ for skeletal electrons and $4N + 2$ for valence electrons (N represents the number of vertexes).[10,11] Over the course of several decades, a unified electron-counting rule for bonding electrons was developed by Jemmis et al.[12,13] This rule encompasses the Wade rule as a special case and aids in understanding the stability of fused boranes, carboranes, and metallaboranes. Recently, 3D aromaticity in *closo* and *nido* boranes has been confirmed, and the exploration of the 3D aromaticity of the dodecaiodo-dodecaborate cluster has indicated the presence of single, rather than double, 3D aromaticity due to its energy instability.[14,15] 3D aromaticity has been also observed in charged or neutral fullerenes, which exhibit the maximum aromaticity when the number of conjugated π electrons follows Hirsch's $2(N + 1)^2$ rule for spherical aromaticity (Figure 1).[16−19] Additionally, Solà and Poater proposed the $2N^2 + 2N + 1$ ($S = N + 1/2$) rule, which is suitable for open-shell spherical aromatic compounds and demonstrated that this rule, along with the Baird rule, can be extended to the open-shell jellium model of metal clusters.[20,21] Open-shell aromaticity has also been reported in triplet states of some metallacycles with adaptive aromaticity.[22−24]

The discovery of highly symmetrical multilayered inorganic fullerenes in solid phases has introduced a new model for investigating 3D aromaticity.[25] Subsequently, several typical Zintl clusters with a three-layered endohedral fullerene-like structure and stoichiometries $E@M_{12}@E_{20}$ (E = As, Sn, Sb; M = Cu, Ni, Pd, Au) have been reported in the last two decades. Notable examples include $[As@Ni_{12}@As_{20}]^{3-}$, $[Sb@Pd_{12}@Sb_{20}]^{n-}$, $[Sn@Cu_{12}@Sn_{20}]^{12-}$, and $[K@Au_{12}Sb_{20}]^{5-}$.[26−30] These clusters have been comprehensively investigated, including their interlayer interactions, electronic structure construction, magnetic aromaticity, and isostructural clusters with compositions involving other elements, using quantum chemical calculations.[31−34] Furthermore, in addition to carbon-free fullerenes, the synthesis of ligand-protected inorganic fullerene-like molecules, such as the golden fullerene $[Au_{32}(Ph_3P)_8(dpa)_6]^{2-}$ (Hdpa = 2,2′-bipyridylamine) and $Au_{32}(R_3P)_{12}Cl_8$ (R = Et, ^{n}Pr, ^{n}Bu), has showcased the versatility of synthetic routes (Figure 1).[35,36] Nevertheless, inorganic fullerenes or fullerene-like clusters composed of the heaviest group 15 element Bi have not been isolated yet, despite some reported structures involving corresponding P, As, and Sb elements.[26−28,37]

Received: February 29, 2024
Revised: April 25, 2024
Accepted: April 26, 2024
Published: May 8, 2024

https://doi.org/10.1021/jacs.4c03024
J. Am. Chem. Soc. 2024, 146, 14166−14173

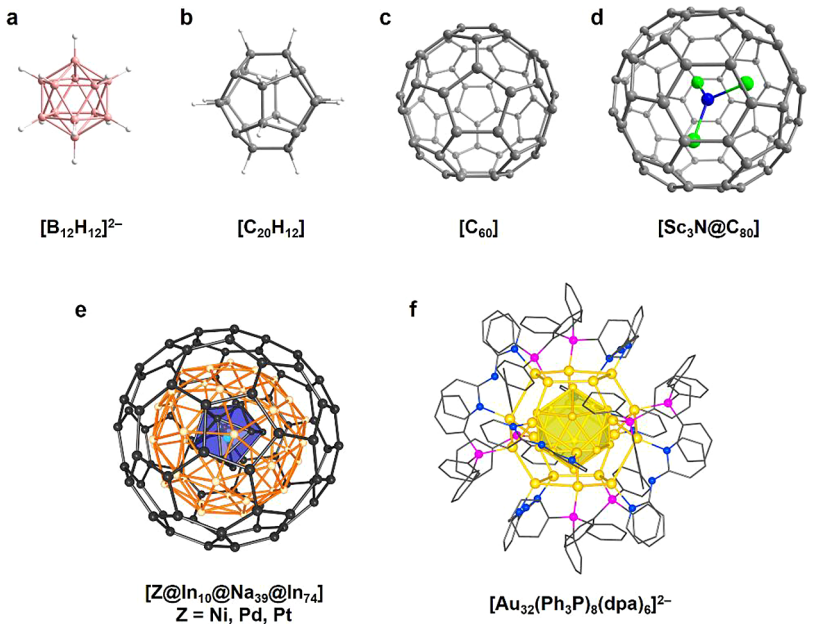

Figure 1. Structures of $[B_{12}H_{12}]^{2-}$ (a), carbon fullerenes (b–d), and fullerene-like inorganic clusters (e,f).

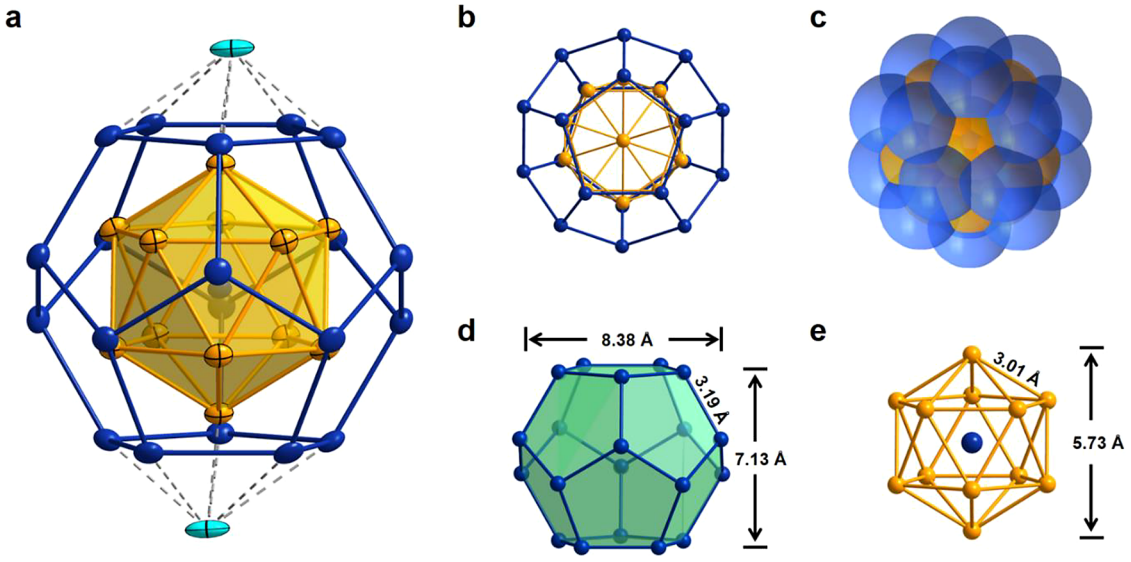

Figure 2. (a) Structure of cluster $[K_2(Bi@Pd_{12}@Bi_{20})]^{4-}$ with thermal ellipsoids drawn at the 50% probability level. (b) Top view of cluster $[Bi@Pd_{12}@Bi_{20}]^{6-}$. (c) Space-filling model of the cluster $[Bi@Pd_{12}@Bi_{20}]^{6-}$. (d) Structure of the $\{Bi_{20}\}$ shell. The bond lengths are the average of all Bi–Bi distances. (e) Structure of the $\{Bi@Pd_{12}\}$ core. The bond lengths are the averages of all Pd–Pd distances.

Polybismuth clusters have attracted considerable attention due to their aromatic behavior and magnetic properties.[38−41] One striking example is cluster $[Th@Bi_{12}]^{4-}$, which exhibits 2π electrons delocalized over the nonplanar $\{Bi_{12}\}$ and displays a ring current as strong as that in porphine, making it an all-metal aromatic compound.[42] The existence of ϕ-aromaticity in the triangular-prismatic $\{Bi_6\}$ cluster has been extensively discussed by chemists.[43,44] However, the synthesis of polybismuth clusters has historically been limited compared with other lighter element congeners. While Zintl detected the potential existence of the Bi_7^{3-} anion through potentiometric titration experiments in 1932, Bi_2^{2-} and Bi_4^{2-} were the largest known bismuth anion clusters for an extended period.[45−48] It was not until 2014 that Dehnen and co-workers successfully isolated Bi_{11}^{3-} from the solution phase, overcoming this limitation.[49] Currently reported bismuth anion clusters mostly adopt polycyclic structures or only contain small fragments of Bi, such as $[Ge_4Bi_{14}]^{4-}$ and $[Ga_2Bi_{16}]^{4-}$ with $\{Bi_7\}$ fragments.[50−55] Despite the existence of some Bi-containing cage-like cationic clusters and ternary anionic clusters, polybismuth clusters with high-symmetry cage-like structures are yet to be synthesized.[56−64]

In this contribution, we present the synthesis and structure of a ternary cluster $[K_2(Bi@Pd_{12}@Bi_{20})]^{4-}$, featuring an onion-like $[Bi@Pd_{12}@Bi_{20}]^{6-}$ core coordinated with two K^+ cations through electrostatic interactions. The electronic structure of $[K_2(Bi@Pd_{12}@Bi_{20})]^{4-}$, analyzed via density of states, reveals bonding and antibonding orbitals resembling superatomic shells. Calculated 3D NICS values for the overall cluster exhibit a continuous shielding region of ±5.0 ppm at 6.0 Å

https://doi.org/10.1021/jacs.4c03024
J. Am. Chem. Soc. 2024, 146, 14166−14173

from the cluster center. Combined with the EDDB analysis results for the delocalized electrons, the $[Bi@Pd_{12}@Bi_{20}]^{6-}$ cluster demonstrates the open-shell aromatic characteristic.

RESULTS AND DISCUSSION

The compound was prepared by the reaction of K_5Bi_4 and $Pd(PPh_3)_4$ (Ph = phenyl) in N,N-dimethylformamide at 60 °C, using crypt-2.2.2 (4,7,13,16,21,24-hexaoxa-1,10-diazabicyclo[8.8.8]hexacosane) as a chelating agent. Following centrifuging and layering of the reaction solution with toluene, block-like crystals were isolated after 1 week and characterized as $[K(crypt\text{-}2.2.2)]_4[K_2(Bi@Pd_{12}@Bi_{20})]\cdot 2DMF\cdot 2tol$ by single-crystal X-ray diffraction. The K: Pd: Bi ratio was further confirmed by EDX (energy-dispersive X-ray spectroscopy). The anion $[K_2(Bi@Pd_{12}@Bi_{20})]^{4-}$ (**1**), which shows slight deviations from C_{2h} symmetry, consists of an onion-skin-like $[Bi@Pd_{12}@Bi_{20}]^{6-}$ cluster (**1a**) and two K^+ cations that cap two opposite pentagonal faces of $\{Bi_{20}\}$.

While two prominent examples of pnictogen clusters with a three-layer nested structure, namely, $[As@Ni_{12}@As_{20}]^{3-}$ and $[Sb@Pd_{12}Sb_{20}]^{3-/4-}$, have been previously isolated, the synthesis of the corresponding bismuth analogue remains challenging due to its sensitivity and instability.[26−29] Cluster **1a**, exhibiting nearly perfect I_h point symmetry, can be described as a pentagonal dodecahedral $\{Bi_{20}\}$ encapsulating an endohedral icosahedral $\{Bi@Pd_{12}\}$, with the Pd atoms positioned below the pentagonal planes of $\{Bi_{20}\}$, as illustrated in Figure 2. The Bi−Bi bond lengths within $\{Bi_{20}\}$ of cluster **1a** are observed to fall within a narrow range of 3.1836(10)−3.2278(10) Å, which are notably longer than the sum of single-bond covalent radii of bismuth (3.02 Å) as well as those found in bismuth Zintl clusters (2.9164(14)−3.0292(15) Å in $[Bi_{11}]^{3-}$) and Bi_2Ph_4 (2.990 Å).[50,63] This phenomenon of the bond elongation within dodecahedral cages has been previously observed in reported $[E@M_{12}@E_{20}]^{n-}$ (E = Sn, As, Sb; M = Cu, Ni, Pd).[26−29]

In comparison to the Pd−Bi contacts between the $\{Bi_{20}\}$ shell and $\{Bi@Pd_{12}\}$ core ranging from 2.7615(18) and 2.8291(16) Å, the Pd−Bi bond lengths to the central Bi atom are slightly longer and fall within a narrow range of 2.8531(14)−2.8791(12) Å. The Pd−Pd distances in **1** (2.9850(2)−3.0343(18) Å) are consistent with those observed in $[Sb@Pd_{12}@Sb_{20}]^{3-/4-}$ (3.003(10) Å and 3.0009(5) Å, av), which suggests that variations in the composition of the external dodecahedron and central atom have a minor impact on the size of the $\{Pd_{12}\}$ cluster.[28] A unique example of a 14-vertex Zintl ion with multinuclear Pd atoms embedded in a cage containing the Bi element was reported as $[Pd_3Sn_8Bi_6]^{4-}$, in which the Pd−Pd (2.756(2)−2.774(2) Å) and Pd−Bi (2.728(2)−2.752(2) Å) bonds are shorter than those in **1**.[64]

The coordination of two K^+ cations plays a pivotal role in stabilizing cluster **1a**. It is interesting to note that the position of K^+ is not directly above the pentagonal $\{Bi_5\}$ ring, resulting in significant variations in K−Bi contacts ranging from 3.100(5) to 3.642(5) Å. Additionally, the K−Pd distance measures 2.700(4) Å, which is shorter than those observed in various known organometallic and inorganic compounds (>3.2 Å), indicating stronger K−Pd interactions within the anion **1**. In the comparison, the shortest distances between alkali metal cations and Cu atoms in solid phase $A_{12}Cu_{12}Sn_{21}$ are 3.196(7) Å for Na−Cu and 3.578(3) Å for K−Cu, suggesting electrostatic interactions between the alkali metal atoms and $[Sn@Cu_{12}@Sn_{20}]^{12-}$ clusters.[29] Furthermore, it has been proven in the literature that unchelated alkali metal ions can serve as stabilizing agents for highly negatively charged anionic clusters, aiding in their crystallization. A striking example is the sandwich-type cluster $\{[K_2ZnSn_8(ZnMes)]_2\}^{4-}$, in which four K^+ cations bridge two identical $[ZnSn_8(ZnMes)]$ units.[65] According to the results of the energy decomposition analysis (EDA), we consider the K−Pd and K−Bi contacts of **1** as electrostatic interactions, as elaborated below. Variable temperature direct current (dc) susceptibility measurements were carried out on a crystallized sample of $[K(crypt\text{-}2.2.2)]_4[K_2Pd_{12}Bi_{21}]\cdot 2DMF\cdot 2tol$. The effective magnetic moment (μ_{eff}) values exhibited a gradual decrease as the temperature decreased, from 3.32 μ_B at 300 K to 0.89 μ_B at 2 K (Figure S6).

The electronic structure of $[K_2(Bi@Pd_{12}Bi_{20})]^{4-}$ was further explored via the density of states (DOS), in order to locate the contribution from the different electronic shells from the outer Bi_{20} dodecahedron, embedded Pd_{12} icosahedron, the central Bi atom, and the capping K atoms (Figure 3). The computationally explored spin-states show an energy difference between doublet and quartet of 3.8 kcal/mol for $[Bi@Pd_{12}@Bi_{20}]^{6-}$ and 2.1 kcal/mol for $[K_2(Bi@Pd_{12}@Bi_{20})]^{4-}$ favoring the doublet spin-state (Table S5), which denotes crystal packing effects on determining the cluster spin-state. Thus, a quartet spin-state is preferred as given by μ_{eff} and effects of the crystal lattice for the overall cluster and thus discussed hereafter. The electron count given by Bi + 12 × Pd + 20 × Bi + 2 × K + 4 = 5e + 12 × 0e + 20 × 5e + 2 × 1e + 4e = 111 ve leads a related electronic shell structure to the 108-*ve* $[Sn@Cu_{12}@Sn_{20}]^{12-}$ cluster given by

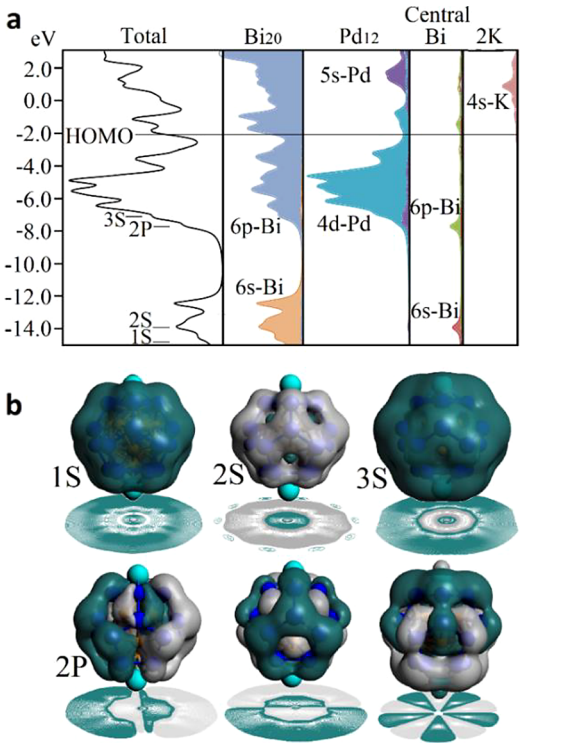

Figure 3. (a) Total density of states (Total), and partial density of states for the contribution from Bi_{20}, Pd_{12}, central Bi, and capping K atoms. (b) Isosurfaces for selected superatomic shells with contribution from central Bi atom, and related countour plots at the equatorial plane to denote the bonding/antibonding multilayer characteristics.

https://doi.org/10.1021/jacs.4c03024
J. Am. Chem. Soc. 2024, 146, 14166−14173

$1S^2 2S^2 1P^6 1D^{10} 1F^{14} 1G^{18} 2P^6 1H^6 2D^{10} 3S^2 1H^{10} 2F^8 1I^8 3P^6$ (108-*ve*) with an additional of partially occupied $1I^3$ shell (111-*ve*), where F, G, and higher angular momentum shells are split by symmetry.[29] The atomic 6s-Bi shell of the central atom contributes to low-lying molecular orbitals, in the region of the 6s-Bi manifold from the Bi_{20} dodecahedron, with a slight contribution from the 5s-Pd of Pd_{12} icosahedron. This combination leads to a bonding orbital within the overall cluster, which resembles a totally symmetric superatomic 1S-shell, followed by an antibonding $Bi-Pd_{12}Bi_{20}$ combination as a superatomic 2S-shell, similar to those of the $[Sn@Cu_{12}@Sn_{20}]^{12-}$ cluster.[29,33] The atomic 6p-Bi shell of the central atom relies on the region contributed mainly by 4d-Pd and 6p-Bi shells of both icosahedral and dodecahedral cages, respectively, resulting in a superatomic 2P shell. Note that the 1P shell is contributed mainly by 6s-Bi shells from the dodecahedron, located below. Moreover, the frontier orbitals are contributed by both icosahedral and dodecahedral layers, as given by the isosurface plot of HOMO and LUMO (Figure S8). Hence, the central Bi atom ensures a filled $6s^2 6p^6$ electronic configuration, given by the bonding contribution from the external shells. Thus, such a feature suggests a plausible spherical aromatic behavior. Charge distribution analysis from EDDB calculations denotes the central Bi atom to carry a −0.86e in $[Bi@Pd_{12}]^{3-}$ species, whereas the charge of the $[Bi@Pd_{12}]$ unit is −1.20e and that of the Bi_{20} layer is −4.80e. Similar results were obtained from electron difference maps between the $[Bi@Pd_{12}]^{3-}$ and $[Bi_{20}]^{3-}$ layers (Figure S9), where charge accumulation is denoted at the outer dodecahedral layer. The spin-density distribution in the overall cluster exposes that the unpaired electrons of $[K_2(Bi@Pd_{12}Bi_{20})]^{4-}$ are distributed mainly along the outer Bi_{20} layer (Figure S8).

The interaction energy per each capping K atom is evaluated at the molecular level via an energy decomposition analysis (EDA) from the K^+-$[KPd_{12}Bi_{21}]^{5-}$ fragmentation scheme in which the $[KPd_{12}Bi_{21}]^{5-}$ fragment is a quartet.[66,67] The obtained results suggest an interaction energy of −287.4 kcal/mol, which is stabilized mainly by the electrostatic character of the interaction (89.4%), followed by a slight contribution (9.7%) from orbital interactions, and to a lesser extent from the London dispersion character (0.9%). Thus, the K cap is aggregated to the $[Pd_{12}Bi_{21}]^{6-}$ multilayer cluster by electrostatic interactions. Such results are similar to those obtained for the interaction of aromatic dimetalla[10]-annulenes and alkali metals, suggesting that in both planar and spherical aromatic species alkali metals are part of the overall structure in addition to being considered as counterions, leading to a tune in the overall aromatic characteristics of the main structure.[65]

To further evaluate spherical aromatic characteristics, the resulting shielding/deshielding response enabled under an external magnetic field is obtained as an isosurface representation of NICS values accounting for the orientation-averaged (isotropic) response as a result of the constant molecular tumbling in solution (Figure 4). The calculated values for $[K_2(Bi@Pd_{12}@Bi_{20})]^{4-}$ exhibit a continuous shielding region ascribed to the cluster contour which is ±5.0 ppm at 6.0 Å from the center of the cluster. Such a feature is inherent to the spherical aromatic behavior, owing that the orientation-averaged response is of an overall shielding character.[68,69] Under a specific orientation of the external field, a long-range shielding region of −5.0 ppm at 12.2 Å along the $K-Pd_{12}Bi_{21}-K$ axis (B_z^{ind}) from the center of the cluster, and

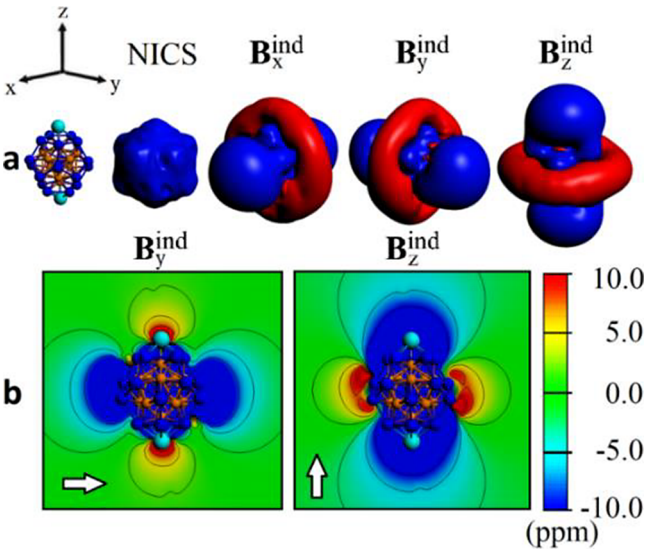

Figure 4. (a) Three-dimensional representations of the NICS values accounting for the orientational-averaged values (isotropic). (b) Specific orientations of the applied field. Isosurface set at ±2.0 ppm, blue: shielding; red, deshielding.

of −5.0 ppm at 11.7 Å from *x*- and *y*-axis (B_x^{ind}, B_y^{ind}), with a complementary deshielding region oriented perpendicularly to the shielding cone. Such property is inherent to spherical aromatic compounds, which in contrast to planar aromatics enables a shielding cone property from different orientations of the external field.[70−72] Hence, the $[K_2(Bi@Pd_{12}@Bi_{20})]^{4-}$ cluster is ascribed to a heavy spherical aromatic multilayer structure. For comparison purposes, the related $E@M_{12}@E_{20}$ species given by $[As@Ni_{12}@As_{20}]^{3-}$ and $[Sb@Pd_{12}@Sb_{20}]^{3-/4-}$ were evaluated in terms of aromaticity from the characteristics of the resulting long-range shielding cone, owing to the central atom avoids evaluation from an inner probe. In this sense, at 8.0 Å from the center, shielding values of −10.9 ppm are found for doublet $^2[K_2(Bi@Pd_{12}@Bi_{20})]^{4-}$ cluster, and of −19.8 ppm in its quadruplet spin-state ($^4[K_2(Bi@Pd_{12}@Bi_{20})]^{4-}$) under a parallel applied magnetic field, denoting a stronger shielding cone ascribed to a stronger aromatic character for the later spin-state. In addition, for $[As@Ni_{12}@As_{20}]^{3-}$ and $[Sb@Pd_{12}@Sb_{20}]^{3-/4-}$, values of −13.2 and −9.9/-7.1 ppm were obtained at 8.0 Å from the center, respectively, suggesting that $^4[K_2(Bi@Pd_{12}@Bi_{20})]^{4-}$ features an enhanced shielding cone accounting for a higher aromatic character.

Moreover, the (resonance) electronic structure is evaluated in terms of the electron density of delocalized bonds (EDDB) to deliver an (unperturbed) electron-density-based approach for unraveling spherical aromatic characteristics.[73] The EDDB approach is employed for the inner palladium icosahedron model without and with the encapsulated closed-shell bismuth trianion (Figure 5a), Pd_{12} and $[Bi@Pd_{12}]^{3-}$, respectively, the outer bismuth dodecahedron model Bi_{20}^{3-} trianion (Figure 5b), and the entire cluster without K cations, $[Bi@Pd_{12}@Bi_{20}]^{6-}$ (Figure 5c). The model clusters $[Bi@Pd_{12}]^{3-}$ (singlet) and Bi_{20}^{3-} (quartet) represent electronically stable ground-state minima with spins and charges that sum to the total spin and charge of $[Bi@Pd_{12}@Bi_{20}]^{6-}$. The results denote that the neutral Pd_{12} model shows significant delocalization of electrons (each Pd atom contributes about 1.31*e* to delocalization, mostly via σ-type conjugation of 4d orbitals), but the inclusion of Bi^{3-} to a large extent affects coherence of the wave function

https://doi.org/10.1021/jacs.4c03024
J. Am. Chem. Soc. 2024, 146, 14166−14173

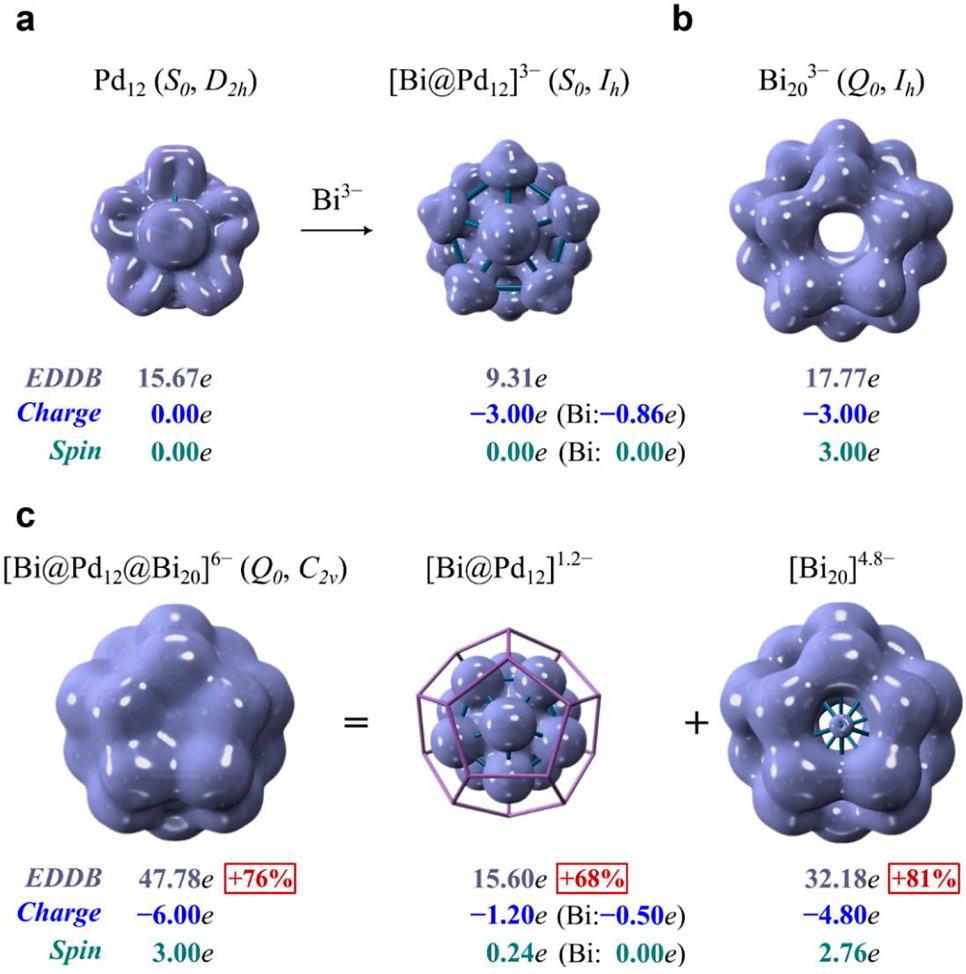

Figure 5. EDDB isosurfaces for Pd_{12} and $[Bi@Pd_{12}]^{3-}$ (a), Bi_{20}^{3-} (b), and $[Bi@Pd_{12}@Bi_{20}]^{6-}$ (c) with the corresponding EDDB-based populations of delocalized electrons, total/fragment charges, and spins.

as the EDDB populations drop from 15.67*e* to 9.31*e*. Destructive interference of molecular orbitals of Pd_{12} and Bi^{3-} is also reflected by the decrease of the sum of Wiberg's bond orders (WBO) between palladium atoms from 8.35 in Pd_{12} to 4.19 in $[Bi@Pd_{12}]^{3-}$. Interestingly, this may have no negative effect on the stability/integrity of the latter as the inclusion of Bi^{3-} increases the HOMO−LUMO gap from 1.28 to 1.74 eV and it recovers the high symmetry (I_h). This is mainly due to the significant overlap between the 6p subshell (Bi) and $4d_{z2}$ (Pd) atomic orbitals, giving rise to much stronger Pd−Bi bonding (WBO ≈ 0.28) compared to the direct Pd−Pd bonding (WBO ≈ 0.06). It is worth noting that the number of valence electrons of $[Bi@Pd_{12}]^{3-}$ is 128*e*, thus following the $2(N+1)^2$ Hirsch rule for spherical aromaticity with $N = 7$.[16] The relatively low EDDB value of only 9.31*e* delocalized is not unexpected taking into account that Schleyer and co-workers found that the Hirsch rule works better for species with 50 electrons or less.[74] Still, the closed-shell configuration provides stability to the cluster. In turn, the dodecahedron Bi_{20}^{3-} model is electronically stable at its quartet ground state, and according to the EDDB, it shows moderate delocalization of electrons: each Bi atom contributes about 0.89*e* to delocalization, and the average effectiveness of delocalization within the 6p subshell is only 23.0%. Each Bi atom bears a lone pair, and the rest of the 63 valence electrons are distributed in an electronic configuration $h_g^{10}\ t_{2u}^{6}\ a_{1g}^{2}\ h_u^{10}\ t_{1u}^{6}\ g_g^{8}\ h_g^{10}\ g_u^{8}\ t_{1u}^{3}$, which has a half filled with the same spin subshell that brings additional stability (see Figure S7). This configuration is analogous to that of C_{60}^{6-}, which is considered an aromatic species, but with the t_{1u} subshell remaining half-filled.[1] Interestingly, the inclusion of $[Bi@Pd_{12}]^{3-}$ into Bi_{20}^{3-} leads to redistribution of charge toward the bismuth dodecahedron that increases delocalization within both spheres by on average 76%, while spin distribution remains almost unchanged with about 92% of unpaired electrons delocalized over the $[Bi_{20}]$ sphere. Moreover, in $[Bi@Pd_{12}@Bi_{20}]^{6-}$ the effectiveness of delocalization in the 6p subshell of $[Bi_{20}]$ increases to 44.1%, which is comparable to the corresponding effectiveness of the π-electron delocalization in thiophene.[75] Thus, in comparison to the bare Bi_{20}^{3-} layer, the formation of the overall cluster enhances the open-shell spherical aromatic character, in line with the magnetic criteria of aromaticity (*vide supra*). In addition, electron delocalization function (ELF) is provided (Figure S10), which shows an ELF bifurcation value of 0.4 at the outer Bi_{20} layer, denoting, in agreement with EDDB results, moderate electronic delocalization.[76]

CONCLUSIONS

In summary, a K-capped endohedral $[Bi@Pd_{12}@Bi_{20}]^{6-}$ cluster core is characterized as $[K_2(Bi@Pd_{12}@Bi_{20})]^{4-}$, featuring a multilayer structure exploiting the dodecahedron-icosahedron duality, extending such species to heavier inorganic fullerene

https://doi.org/10.1021/jacs.4c03024
J. Am. Chem. Soc. 2024, 146, 14166−14173

realms. The here described cluster exhibits an open-shell spin-state, retaining spherical aromatic characteristics given by their electronic structure and induced magnetic field properties. Interestingly, the $[Bi@Pd_{12}]^{3-}$ and $^4Bi_{20}^{3-}$ units, which are moderately aromatic, combined to form the $[Bi@Pd_{12}@Bi_{20}]^{6-}$ cluster generates a system with higher aromatic character according to the EDDB and three-dimensional representations of the induced magnetic field criteria. It remains to be seen whether such an enhancement of the aromatic character of the cluster with respect to that of its units is a particular property of the $[Bi@Pd_{12}@Bi_{20}]^{6-}$ cluster or if it can be generalized to any metallic endohedral inorganic fullerene.

■ ASSOCIATED CONTENT

Supporting Information

The Supporting Information is available free of charge at https://pubs.acs.org/doi/10.1021/jacs.4c03024.

Detailed experimental procedures, crystallographic supplementation, magnetic susceptibility study, energy-dispersive X-ray (EDX) spectroscopic analysis, and quantum-chemical studies (PDF)

EDDB-based populations of delocalized electrons of $[Bi@Pd_{12}@Bi_{20}]^{6-}$ (MP4)

EDDB-based populations of delocalized electrons of $[Bi_{20}]^{4.8-}$ (MP4)

EDDB-based populations of delocalized electrons of $[Bi@Pd_{12}]^{1.2-}$ (MP4)

Accession Codes

CCDC 2268669 contains the supplementary crystallographic data for this paper. These data can be obtained free of charge via www.ccdc.cam.ac.uk/data_request/cif, or by emailing data_request@ccdc.cam.ac.uk, or by contacting The Cambridge Crystallographic Data Centre, 12 Union Road, Cambridge CB2 1EZ, UK; fax: +44 1223 336033.

■ AUTHOR INFORMATION

Corresponding Author

Zhong-Ming Sun − *State Key Laboratory of Elemento-Organic Chemistry, Tianjin Key Lab for Rare Earth Materials and Applications, School of Materials Science and Engineering, Nankai University, Tianjin 300350, China;* orcid.org/0000-0003-2894-6327; Email: sunlab@nankai.edu.cn

Authors

Cong-Cong Shu − *State Key Laboratory of Elemento-Organic Chemistry, Tianjin Key Lab for Rare Earth Materials and Applications, School of Materials Science and Engineering, Nankai University, Tianjin 300350, China;* orcid.org/0000-0001-7407-3446

Dariusz W. Szczepanik − *K. Guminski Department of Theoretical Chemistry, Faculty of Chemistry, Jagiellonian University, 30-387 Kraków, Poland*

Alvaro Muñoz-Castro − *Facultad de Ingeniería, Arquitectura y Diseño, Universidad San Sebastián, Santiago 8420524, Chile;* orcid.org/0000-0001-5949-9449

Miquel Solà − *Institut de Química Computacional i Catàlisi and Departament de Química, Universitat de Girona, 17003 Girona, Catalonia, Spain;* orcid.org/0000-0002-1917-7450

Complete contact information is available at: https://pubs.acs.org/10.1021/jacs.4c03024

Notes

The authors declare no competing financial interest.

■ ACKNOWLEDGMENTS

This work was supported by the National Natural Science Foundation of China (nos. 92161102, 223B2110, and 22371140), the Natural Science Foundation of Tianjin City (no. 21JCZXJC00140), and 111 project (B18030) from China (MOE). A.M.-C. thanks financial support from ANID FONDECYT Regular 1221676. M.S. thanks the Spanish Ministerio de Ciencia e Innovación for project PID2020-113711GB-I00 and the Generalitat de Catalunya for project 2017SGR39. D.W.S. acknowledges financial support from the National Science Centre, Poland (2021/42/E/ST4/00332). We thank Yu-He Xu for her invaluable contribution to the discussion and revision of the paper.

■ REFERENCES

(1) Garcia-Borràs, M.; Osuna, S.; Luis, J. M.; Swart, M.; Solà, M. The role of aromaticity in determining the molecular structure and reactivity of (endohedral metallo)fullerenes. *Chem. Soc. Rev.* **2014**, *43*, 5089−5105.

(2) Chen, Z.; Jiao, H.; Hirsch, A.; Schleyer, P. v. R. Spherical homoaromaticity. *Angew. Chem., Int. Ed.* **2002**, *41*, 4309−4312.

(3) Chen, Z.; King, R. B. Spherical aromaticity: recent work on fullerenes, polyhedral boranes, and related structures. *Chem. Rev.* **2005**, *105*, 3613−3642.

(4) Solà, M. Aromaticity rules. *Nat. Chem.* **2022**, *14*, 585−590.

(5) King, R. B. Three-dimensional aromaticity in polyhedral coranes and related molecules. *Chem. Rev.* **2001**, *101*, 1119−1152.

(6) Bakouri, O. El.; Szczepanik, D. W.; Jorner, K.; Ayub, R.; Bultinck, P.; Solà, M.; Ottosson, H. Three-Dimensional Fully π-Conjugated Macrocycles: When 3D-Aromatic and when 2D-Aromatic-in-3D? *J. Am. Chem. Soc.* **2022**, *144*, 8560−8575.

(7) Bühl, M.; Hirsch, A. Spherical aromaticity of fullerenes. *Chem. Rev.* **2001**, *101*, 1153−1183.

(8) Lipscomb, W. N.; Pitochelli, A. R.; Hawthorne, M. F. Probable structure of the $B_{10}H_{10}^{-2}$ ion. *J. Am. Chem. Soc.* **1959**, *81*, 5833−5834.

(9) Knoth, W. H.; Miller, H. C.; England, D. C.; Parshall, G. W.; Muetterties, E. L. Derivative chemistry of $B_{10}H_{10}^{-}$ and $B_{12}H_{12}^{-}$. *J. Am. Chem. Soc.* **1962**, *84*, 1056−1057.

(10) Wade, K. The structural significance of the number of skeletal bonding electron-pairs in carboranes, the higher boranes and borane anions, and various transition-metal carbonyl cluster compounds. *J. Chem. Soc. D* **1971**, 792−793.

(11) Mingos, D. M. P. A general theory for cluster and ring compounds of the main group and transition elements. *Nat. Phys. Sci.* **1972**, *236*, 99−102.

(12) Jemmis, E. D.; Balakrishnarajan, M. M.; Pancharatna, P. D. A unifying electron-counting rule for macropolyhedral boranes, metallaboranes, and metallocenes. *J. Am. Chem. Soc.* **2001**, *123*, 4313−4323.

(13) Jemmis, E. D.; Balakrishnarajan, M. M.; Pancharatna, P. D. Electronic requirements for macropolyhedral boranes. *Chem. Rev.* **2002**, *102*, 93−144.

(14) Poater, J.; Viñas, C.; Bennour, I.; Escayola, S.; Solà, M.; Teixidor, F. Too persistent to give up: aromaticity in boron clusters survives radical structural changes. *J. Am. Chem. Soc.* **2020**, *142*, 9396−9407.

(15) Poater, J.; Escayola, S.; Poater, A.; Teixidor, F.; Ottosson, H.; Viñas, C.; Solà, M. Single−not double−3D-aromaticity in an oxidized closo icosahedral dodecaiodo-dodecaborate cluster. *J. Am. Chem. Soc.* **2023**, *145*, 22527−22538.

(16) Hirsch, A.; Chen, Z.; Jiao, H. Spherical aromaticity in I_h symmetrical fullerenes: the $2(N+1)^2$ rule. *Angew. Chem., Int. Ed.* **2000**, *39*, 3915−3917.

(17) Kroto, H. W.; Heath, J. R.; O'Brien, S. C.; Curl, R. F.; Smalley, R. E. C_{60}: buckminsterfullerene. *Nature* **1985**, *318*, 162−163.
(18) Stevenson, S.; Rice, G.; Glass, T.; Harich, K.; Cromer, F.; Jordan, M. R.; Craft, J.; Hadju, E.; Bible, R.; Olmstead, M. M.; Maitra, K.; Fisher, A. J.; Balch, A. L.; Dorn, H. C. Small-bandgap endohedral metallofullerenes in high yield and purity. *Nature* **1999**, *401*, 55−57.
(19) Hirsch, A.; Chen, Z.; Jiao, H. Spherical aromaticity of inorganic cage molecules. *Angew. Chem., Int. Ed.* **2001**, *40*, 2834−2838.
(20) Poater, J.; Solà, M. Open-shell spherical aromaticity: the $2N^2$ + 2N + 1 (with S = N + 1/2) rule. *Chem. Commun.* **2011**, *47*, 11647−11649.
(21) Poater, J.; Solà, M. Open-shell jellium aromaticity in metal clusters. *Chem. Commun.* **2019**, *55*, 5559−5562.
(22) Shen, T.; Chen, D.; Lin, L.; Zhu, J. Dual aromaticity in both the T_0 and S_1 states: osmapyridinium with phosphonium substituents. *J. Am. Chem. Soc.* **2019**, *141*, 5720−5727.
(23) Chen, D.; Szczepanik, D. W.; Zhu, J.; Sola, M. Probing the origin of adaptive aromaticity in 16-valence-electron metallapentalenes. *Chem. − Eur. J.* **2020**, *26*, 12964−12971.
(24) Ye, Q.; Fang, Y.; Zhu, J. Adaptive aromaticity in 18e metallapentalenes. *Inorg. Chem.* **2023**, *62*, 14764−14772.
(25) Sevov, S. C.; Corbett, J. D. Carbon-free fullerenes: condensed and stuffed anionic examples in indium systems. *Science* **1993**, *262*, 880−883.
(26) Moses, M. J.; Fettinger, J. C.; Eichhorn, B. W. Interpenetrating As_{20} fullerene and Ni_{12} icosahedra in the onion-skin $[As@Ni_{12}@As_{20}]^{3-}$ ion. *Science* **2003**, *300*, 778−780.
(27) Li, Z.; Ruan, H.; Wang, L.; Liu, C.; Xu, L. Counterion-induced crystallization of intermetalloid Matryoshka clusters $[Sb@Pd_{12}@Sb_{20}]^{3-,4-}$. *Dalton Trans.* **2017**, *46*, 3453−3456.
(28) Wang, Y.; Moses-DeBusk, M.; Stevens, L.; Hu, J.; Zavalij, P.; Bowen, K.; Dunlap, B. I.; Glaser, E. R.; Eichhorn, B. $Sb@Ni_{12}@Sb_{20}^{\mp}$ and $Sb@Pd_{12}@Sb_{20}^{n}$ cluster anions, where n = +1,−1,−3,−4: multi-oxidation-state clusters of interpenetrating platonic solids. *J. Am. Chem. Soc.* **2017**, *139*, 619−622.
(29) Stegmaier, S.; Fässler, T. F. A bronze matryoshka: the discrete intermetalloid cluster $[Sn@Cu_{12}@Sn_{20}]^{12-}$ in the ternary phases $A_{12}Cu_{12}Sn_{21}$ (A = Na, K). *J. Am. Chem. Soc.* **2011**, *133*, 19758−19768.
(30) Xu, Y.; Tian, W.; Muñoz-Castro, A.; Frenking, G.; Sun, Z. An all-metal fullerene: $[K@Au_{12}Sb_{20}]^{5-}$. *Science* **2023**, *382*, 840−843.
(31) Kulichenko, M.; Fedik, N.; Boldyrev, A.; Muñoz-Castro, A. Expansion of magnetic aromaticity criteria to multilayer structures: magnetic response and spherical aromaticity of matryoshka-like cluster $[Sn@Cu_{12}@Sn_{20}]^{12-}$. *Chem. − Eur. J.* **2020**, *26*, 2263−2268.
(32) Carey, D. M.; Morales-Verdejo, C.; Muñoz-Castro, A. $[As@Ni_{12}@As_{20}]^{3-}$ and $[Sn@Cu_{12}@Sn_{20}]^{12-}$ clusters. Related structures with different construction philosophy. *Chem. Phys. Lett.* **2015**, *638*, 99−102.
(33) Rauhalahtib, M.; Muñoz-Castro, A. Interaction in multilayer clusters: a theoretical survey of $[Sn@Cu_{12}@Sn_{20}]^{12-}$, a three-layer matryoshka-like intermetalloid. *RSC Adv.* **2015**, *5*, 18782−18787.
(34) Chang, Ch.; Patzer, A. B. C.; Sedlmayr, E.; Sülzle, D.; Steinke, T. Onion-like inorganic fullerenes of icosahedral symmetry. *Comput. Mater. Sci.* **2006**, *35*, 387−390.
(35) Yuan, S.; Xu, C.; Li, J.; Wang, Q. Ligand-protected "golden fullerene": the dipyridylamido $[Au_{32}]^{8+}$ nanocluster. *Angew. Chem., Int. Ed.* **2019**, *58*, 5906−5909.
(36) Kenzler, S.; Fetzer, F.; Schrenk, C.; Pollard, N.; Frojd, A. R.; Clayborne, A. Z.; Schnepf, A. Synthesis and characterization of three multi-shell metalloid gold clusters $Au_{32}(R_3P)_{12}Cl_8$. *Angew. Chem., Int. Ed.* **2019**, *58*, 5902−5905.
(37) Bai, J.; Virovets, A. V.; Scheer, M. Synthesis of inorganic fullerene-like molecules. *Science* **2003**, *300*, 781−783.
(38) Pang, Y.; Nöthling, N.; Leutzsch, M.; Kang, L.; Bill, E.; Gastel, M. V.; Reijerse, E.; Goddard, R.; Wagner, L.; SantaLucia, D.; DeBeer, S.; Neese, F.; Cornella, J. Synthesis and isolation of a triplet bismuthinidene with a quenched magnetic response. *Science* **2023**, *380*, 1043−1048.
(39) Wu, M.; Chen, W.; Wang, D.; Chen, Y.; Ye, S.; Tan, G. Triplet bismuthinidenes featuring unprecedented giant and positive zero field splittings. *Natl. Sci. Rev.* **2023**, *10*, nwad169.
(40) Zhang, P.; Benner, F.; Chilton, N. F.; Demir, S. Organometallic lanthanide bismuth cluster single-molecule magnets. *Chem.* **2022**, *8*, 717−730.
(41) Zhang, P.; Nabi, R.; Staab, J. K.; Chilton, N. F.; Demir, S. Taming super-reduced Bi_2^{3-} radicals with rare earth cations. *J. Am. Chem. Soc.* **2023**, *145*, 9152−9163.
(42) Eulenstein, A. R.; Franzke, Y. J.; Lichtenberger, N.; Wilson, R. J.; Deubner, H. L.; Kraus, F.; Clérac, R.; Weigend, F.; Dehnen, S. Substantial π-aromaticity in the anionic heavy-metal cluster $[Th@Bi_{12}]^{4-}$. *Nat. Chem.* **2021**, *13*, 149−155.
(43) Peerless, B.; Schmidt, A.; Franzke, Y. J.; Dehnen, S. φ-aromaticity in prismatic $\{Bi_6\}$-based clusters. *Nat. Chem.* **2023**, *15*, 347−356.
(44) Szczepanik, D. W.; Solà, M. Does φ-aromaticity exist in prismatic $\{Bi_6\}$-based clusters?. *ChemRxiv* **2023**, DOI: 10.26434/chemrxiv-2023-dkvdg-v2.
(45) Zintl, E.; Dullenkopf, W. Metals and alloys. III. Polyantimonides, polybismuthides and their transformation into alloys. *Z. Phys. Chem.* **1932**, *16*, 183−194.
(46) Xu, L.; Bobev, S.; El-Bahraoui, J.; Sevov, S. C. A naked diatomic molecule of bismuth, $[Bi_2]^{2-}$, with a short Bi-Bi bond: synthesis and structure. *J. Am. Chem. Soc.* **2000**, *122*, 1838−1839.
(47) Gascoin, F.; Sevov, S. C. Synthesis and characterization of A_3Bi_2 (A = K, Rb, Cs) with isolated diatomic dianion of bismuth $[Bi_2]^{2-}$, and an extra delocalized electron. *J. Am. Chem. Soc.* **2000**, *122*, 10251−10252.
(48) Cisar, A.; Corbett, J. D. Polybismuth anions. Synthesis and crystal structure of a salt of the tetrabismuthide(2-) ion, Bi_4^{2-}. A basis for the interpretation of the structure of some complex intermetallic phases. *Inorg. Chem.* **1977**, *16*, 2482−2487.
(49) Weinert, B.; Eulenstein, A. R.; Ababei, R.; Dehnen, S. Formation of $[Bi_{11}]^{3-}$, A homoatomic, polycyclic bismuth polyanion, by pyridine-assisted decomposition of $[GaBi_3]^{2-}$. *Angew. Chem., Int. Ed.* **2014**, *53*, 4704−4708.
(50) Perla, L. G.; Oliver, A. G.; Sevov, S. C. Bi_7^{3-}: The missing family member, finally isolated and characterized. *Inorg. Chem.* **2015**, *54*, 872−875.
(51) Wilson, R. J.; Dehnen, S. $(Ge_4Bi_{14})^{4-}$: A case of "Element Segregation" on the molecular level. *Angew. Chem., Int. Ed.* **2017**, *56*, 3098−3102.
(52) Pan, F.; Wei, S.; Guggolz, L.; Eulenstein, A. R.; Tambornino, F.; Dehnen, S. Insights into formation and relationship of multimetallic clusters: on the way toward Bi-rich nanostructures. *J. Am. Chem. Soc.* **2021**, *143*, 7176−7188.
(53) Mayer, K.; Dums, J. V.; Benda, C. B.; Klein, W.; Fässler, T. F. Solvate-induced semiconductor to metal transition: flat $^1_\infty[Bi^{1-}]$ zigzag chains in metallic $KBi{\cdot}NH_3$ versus $^1_\infty[Bi^{1-}]$ helices in semiconducting KBi. *Angew. Chem., Int. Ed.* **2020**, *59*, 6800−6805.
(54) Heine, J.; Peerless, B.; Dehnen, S.; Lichtenberg, C. Charge makes a difference: molecular ionic bismuth compounds. *Angew. Chem., Int. Ed.* **2023**, *135*, No. e202218771.
(55) Goicoechea, J. M.; Hull, M. W.; Sevov, S. C. Heteroatomic deltahedral clusters: synthesis and structures of *closo*-$[Bi_3Ni_4(CO)_6]^{3-}$, *closo*-$[Bi_4Ni_4(CO)_6]^{2-}$, the open cluster $[Bi_3Ni_6(CO)_9]^{3-}$, and the intermetalloid *closo*-$[Ni_x@\{Bi_6Ni_6(CO)_8\}]^{4-}$. *J. Am. Chem. Soc.* **2007**, *129*, 7885−7893.
(56) Hershaft, A.; Corbett, J. D. The crystal structure of bismuth subchloride. Identification of the ion Bi_9^{5+}. *Inorg. Chem.* **1963**, *2*, 979−985.
(57) Krebs, B.; Hucke, M.; Brendel, C. J. Structure of the Octabismuth(2+) Cluster in Crystalline $Bi_8(AlCl_4)_2$. *Angew. Chem., Int. Ed. Engl.* **1982**, *21*, 445−446.
(58) Ruck, M.; Hampel, S. Stabilization of homonuclear Bi_5^+ and Bi_6^{2+} polycations by cluster anions in the crystal structures of $Bi_{12-x}IrCl_{13-x}$, $Bi_{12-x}RhCl_{13-x}$ and $Bi_{12-x}RhBr_{13-x}$. *Polyhedron* **2002**, *21*, 651−656.

(59) Ruck, M.; Dubenskyy, V.; Söhnel, T. Structure and bonding of Pd@$[Bi_{10}]^{4+}$ in the subbromide $Bi_{14}PdBr_{16}$. *Angew. Chem., Int. Ed.* **2003**, *42*, 2978−2982.
(60) Wahl, B.; Kloo, L.; Ruck, M. The molecular cluster $[Bi_{10}Au_2](SbBi_3Br_9)_2$. *Angew. Chem., Int. Ed.* **2008**, *47*, 3932−393.
(61) Pan, F.; Peerless, B.; Dehnen, S. Bismuth-based metal clusters—from molecular aesthetics to contemporary materials science. *Acc. Chem. Res.* **2023**, *56*, 1018−1030.
(62) Lichtenberger, N.; Wilson, R. J.; Eulenstein, A. R.; Massa, W.; Clérac, R.; Weigend, F.; Dehnen, S. Main group metal−actinide magnetic coupling and structural response upon U^{4+} inclusion into Bi, Tl/Bi, or Pb/Bi cages. *J. Am. Chem. Soc.* **2016**, *138*, 9033−9036.
(63) Calderazzo, F.; Morvillo, A.; Pelizzi, G.; Poli, R. Synthesis and crystal and molecular structure of tetraphenyldibismuthine, Bi_2Ph_4, the first crystallographically characterized tetraorganyl derivative of bismuth(II). *J. Chem. Soc. Chem. Commun.* **1983**, 507−508.
(64) Lips, F.; Clérac, R.; Dehnen, S. $[Pd_3Sn_8Bi_6]^{4-}$: A 14-vertex Sn/Bi cluster embedding a Pd_3 triangle. *J. Am. Chem. Soc.* **2011**, *133*, 14168−14171.
(65) Xu, H.; Tkachenko, N. V.; Muñoz-Castro, A.; Boldyrev, A. I.; Sun, Z. $[Sn_8]^{6-}$-bridged mixed-valence Zn^{I}/Zn^{II} in $\{[K_2ZnSn_8(ZnMes)]_2\}^{4-}$ inverse sandwich-type cluster supported by a Zn^{I}−Zn^{I} bond. *Angew. Chem., Int. Ed.* **2021**, *60*, 9990−9995.
(66) Bickelhaupt, F. M.; Baerends, E. J. Kohn−Sham density functional theory: predicting and understanding chemistry. In *Reviews in computational chemistry*; Lipkowitz, K. B.; Boyd, D. B., Eds.; Wiley, 2000; Vol. *15*, pp 1−86.
(67) Frenking, G.; Bickelhaupt, F. M. The EDA perspective of chemical bonding. In *The chemical bond: fundamental aspects of chemical bonding*; Wiley-VCH Verlag GmbH: Weinheim, 2014; Vol. *1*, pp 121−157.
(68) An, K.; Shen, T.; Zhu, J. Craig-type möbius aromaticity and antiaromaticity in dimetalla[10]annulenes: A metal-induced yin-and-yang pair. *Organometallics.* **2017**, *36*, 3199−3204.
(69) Tkachenko, N. V.; Popov, I. A.; Kulichenko, M.; Fedik, N.; Sun, Z.; Muñoz-Castro, A.; Boldyrev, A. I. Bridging aromatic/antiaromatic units: recent advances in aromaticity and antiaromaticity in main-group and transition-metal clusters from bonding and magnetic analyses. *Eur. J. Inorg. Chem.* **2021**, *2021* (41), 4239−4250.
(70) Schleyer, P. R. V.; Jiao, H. What is aromaticity? *Pure Appl. Chem.* **1996**, *68*, 209−218.
(71) Islas, R.; Heine, T.; Merino, G. The induced magnetic field. *Acc. Chem. Res.* **2012**, *45*, 215−228.
(72) Muñoz-Castro, A. The shielding cone in spherical aromatic structures: insights from models for spherical $2(N + 1)^2$ aromatic fullerenes. *Phys. Chem. Chem. Phys.* **2017**, *19*, 12633−12636.
(73) Szczepanik, D. W.; Andrzejak, M.; Dyduch, K.; Żak, E.; Makowski, M.; Mazurb, G.; Mrozek, J. A uniform approach to the description of multicenter bonding. *Phys. Chem. Chem. Phys.* **2014**, *16*, 20514−20523.
(74) Chen, Z.; Wu, J. I.; Corminboeuf, C.; Bohmann, J.; Lu, X.; Hirsch, A.; Schleyer, P. V. R. Is C_{60} buckminsterfullerene aromatic? *Phys. Chem. Chem. Phys.* **2012**, *14*, 14886−14891.
(75) Szczepanik, D. W.; Andrzejak, M.; Dominikowska, J.; Pawełek, B.; Krygowski, T. M.; Szatylowicz, H.; Solà, M. The electron density of delocalized bonds (EDDB) applied for quantifying aromaticity. *Phys. Chem. Chem. Phys.* **2017**, *19*, 28970−28981.
(76) Santos, J. C.; Andres, J.; Aizman, A.; Fuentealba, P. An aromaticity scale based on the topological analysis of the electron localization function including σ and π contributions. *J. Chem. Theory. Comput.* **2005**, *1*, 83−86.

https://doi.org/10.1021/jacs.4c03024
J. Am. Chem. Soc. 2024, 146, 14166−14173